Thin-Walled Structures 135 (2019) 329–340

Contents lists available at ScienceDirect

Thin-Walled Structures

journal homepage: www.elsevier.com/locate/tws

Full length article

Free vibration behavior of Ti-6Al-4V sandwich beams with corrugated channel cores: Experiments and simulations

Xin Wang[a,c,d,1], Zhen-Yu Zhao[a,c,d,1], Lang Li[a,c,d], Zhi-Jia Zhang[a,d], Qian-Cheng Zhang[a,b,d,*], Bin Han[e,f], Tian Jian Lu[a,c,d,*]

[a] State Key Laboratory for Strength and Vibration of Mechanical Structures, Xi'an Jiaotong University, Xi'an 710049, China
[b] Key Laboratory of Intense Dynamic Loading and Effect, Xi'an, 710024, China
[c] State Key Laboratory of Mechanics and Control of Mechanical Structures, Nanjing University of Aeronautics and Astronautics, Nanjing 210016, China
[d] Nanjing Center for Multifunctional Lightweight Materials and Structures (MLMS), Nanjing University of Aeronautics and Astronautics, Nanjing 210016, PR China
[e] School of Mechanical Engineering, Xi'an Jiaotong University, Xi'an 710049, China
[f] School of Engineering, Brown University, Providence, RI 02912, USA

ARTICLE INFO

Keywords:
Sandwich beam
Corrugated channel core
Free vibration
Homogenization method
Modal test

ABSTRACT

Free vibration of ultralight all-metallic (Ti-6Al-4V alloy) sandwich beams with corrugated channel cores was investigated by experiments and finite element (FE) simulations. The natural frequencies and mode shapes were measured and compared with simulations from both three-dimensional model (3D model) and two-dimensional equivalent model (2D model). Predictions of the 2D model agreed well with results obtained from the 3D model and experiments. It was found that for sandwich beams, the topological change from corrugated core to corrugated channel core eliminates the anisotropy of the structural stiffness and suppresses the local modes of vibration. The effect of geometrical parameters on the first natural frequency was also explored. In addition, preliminary assessment of the influence induced by varying the core topology was carried out. The first natural frequency of sandwich beams with corrugated channel cores having an inclination angle $\theta > 45^{\circ}$ is higher than those of sandwich beams constructed with competing core topologies, including tetrahedral, Kagome and pyramidal trusses and hexagonal honeycombs.

1. Introduction

Sandwich structures with periodic lattice cores possess marvelous multi-functional properties which may be harnessed for novel applications in engineering structures. They not only outperform monolithic structures of the same mass in stiffness, strength and shock resistance, but also provide additional features, such as thermal transport [1–3], energy absorption [4–6] and sound insulation [7–9].

As a type of two-dimensional core topology, corrugations employed as sandwich cores have been widely studied including static and dynamic mechanical properties. Under out-of-plane compression, a corrugation was first deformed by stretching of corrugated member and then collapsed by Euler or plastic buckling at a small strain, softening rapidly due to node failure and/or core buckling [10,11]. Rubino et al. [12] found a serious anisotropy of corrugated sandwich beams under foam projectile impact loading. The anisotropy of corrugations existed also existed in vibration problems of sandwich beams [13]. In terms of vibration features, local vibration modes of corrugated sandwich structures were prone to appear even at relatively low frequencies [13]. In order to suppress the local vibration modes, honeycomb and foam were inserted into the corrugated core [13,14], respectively, for the insertion could be regarded as elastic foundation to stabilize the local parts of the corrugations and face sheets. However, the insertion, especially closed-pore metallic foam, blocks the two-dimensional (2D) channel of the corrugation core, thus becoming a serious barrier for active cooling. Consequently, how to modify the core topology of corrugations to achieve the same advantage in vibration properties is an important issue that must be solved.

More recently, inspired by traditional corrugations, i.e., folded plates, Lu et al. [15] proposed a novel sandwich panel with fluid-through corrugated channel core which exhibits enhanced active cooling performance. It was demonstrated that the proposed sandwich panel also has superior out-of-plane compression performance (especially in the low density regime) in comparison with competing

* Corresponding authors at: State Key Laboratory for Strength and Vibration of Mechanical Structures, Xi'an Jiaotong University, Xi'an 710049, China.
E-mail addresses: zqc111999@xjtu.edu.cn (Q.-C. Zhang), tjlu@nuaa.edu.cn (T.J. Lu).
[1] These authors contributed equally to this work.

https://doi.org/10.1016/j.tws.2018.11.008
Received 25 June 2018; Received in revised form 14 September 2018; Accepted 13 November 2018
Available online 27 November 2018
0263-8231/ © 2018 Elsevier Ltd. All rights reserved.

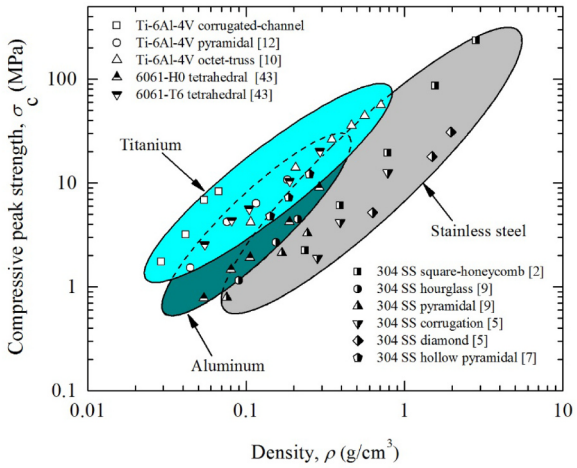

Fig. 1. Excellent out-of-plane compressive strength of sandwich panels with corrugated channel cores [15].

sandwich structures constructed using corrugations, honeycombs and pyramidal trusses as shown in Fig. 1. In other words, the proposed sandwich panels with corrugated channel cores have the capability of simultaneous load bearing and active cooling, attractive for applications in supersonic vehicles, spacecraft skins, cooling jackets for combustors and detonation tubes of pulse detonation engine [16–18]. When such engineering structures are exposed to dynamic loading, the sequent oscillation or vibration may generate serious structural damages if the vibration frequency approaches the natural frequency. For example, as pulse detonation engines (PDEs) are typically subjected to internal moving shock loading, vibration on the detonation tubes may generate various structural damages, e.g., high-cycle fatigue at relatively low pressure, dynamic tearing at medium pressure and even plastic expansion with dynamic fragmentation at high pressure [16]. As the operating frequency of the PDE is usually 40–500 Hz [18–21], it is likely that the corresponding frequency range contains the first two natural frequencies of its sandwich wall [13,14]. Thus, for safety reasons, it is important to investigate the free vibration behavior (natural frequencies and mode shapes) of sandwich beams with corrugated channel cores.

As an important area of concern, free vibration of lightweight sandwich structures has been widely investigated [22–24]. For instance, recent advances in buckling and free vibration of laminated composite and sandwich beams, including theories and finite element simulations, has been comprehensively reviewed [22]. Lou et al. [25,26] studied the free vibration of composite sandwich beams with pyramidal truss cores and considered the effect of local damage on modal characteristics. The modal properties of a clamped-free hexagonal honeycomb plate used for satellite structural design were investigated using experiments, simulations and equivalent approaches [27], while the forced vibration of aluminum and Nomex honeycomb sandwich beams was experimentally studied with clamped-free boundary conditions [28]. Further, the damping characteristics of composite sandwich cylindrical shell with pyramidal truss core were investigated [29], a vibration analysis of multi-span lattice sandwich beams was carried out using the assumed mode method [30], and the free vibration of sandwich beams with soft cores was analyzed based on a refined zig-zag theory [31]. To date, as existing research works on free vibration of sandwich structures have focused mainly upon theories and numerical simulations, experimental investigations are relatively scant.

Among numerous methods [22], homogenization is an effective method to investigate the static or dynamic problems of sandwich structures [32], improving significantly the computational efficiency through simplifying the discrete 2D or 3D lattice core to a homogeneous one [33]. In this study, we employed this method to build an equivalent FE model (2D model) wherein the corrugated channel core was treated as a homogeneous orthotropic core so that the sandwich beam itself could be regarded as a three-layer structure. Correspondingly, the effective elastic constants of the equivalent core were analytically derived.

The outline of this work is as follows. First, a modified fabrication route to form corrugations was detailed and the experimental protocol for modal testing was introduced. Then, global vibration properties of sandwich beams were determined through FE simulations and experiments; meanwhile, a validation study of the 2D model was carried out. Next, the corrugated channel core was compared to traditional corrugations. Further, the influence of key geometrical parameters on free vibration was quantified using FE simulations. Finally, the first natural frequency of sandwich beams with corrugated channel cores was indirectly compared with those of sandwich constructions with competing lattice cores, including tetrahedral, Kagome and pyramidal trusses and hexagonal honeycombs.

2. Experiments

2.1. Materials and fabrication

Fundamental assumptions of the present study are: (1) the behavior of the sandwich falls within the state of small deformation and linear elasticity; (2) local vibration is not considered; (3) no slippage or delamination between the face sheets and the corrugated channel core occurs.

Consider a long, narrow and thin-walled sandwich beam with corrugated channel core as shown in Fig. 2. Relevant geometric parameters are listed as below. The length, width and height of the sandwich beam are L, W and H, respectively. The thickness of the face sheets and the corrugated sheet in the core as well as the height of the core are t_f, t_c and h_c, respectively. The wave amplitude, the length of one-half wave, the corrugated member length, the inclination angle of corrugated member, and the neighboring separation of the core are a, p, l_c, θ and d, respectively. The relative density of the corrugated channel core, $\bar{\rho}$, can thence be expressed as:

$$\bar{\rho} = \frac{t_c l_c}{pd} \tag{1}$$

Ti-6Al-4V has much higher specific yield strength and service temperature than aluminum alloys. Zhao et al. [15] proposed a detailed

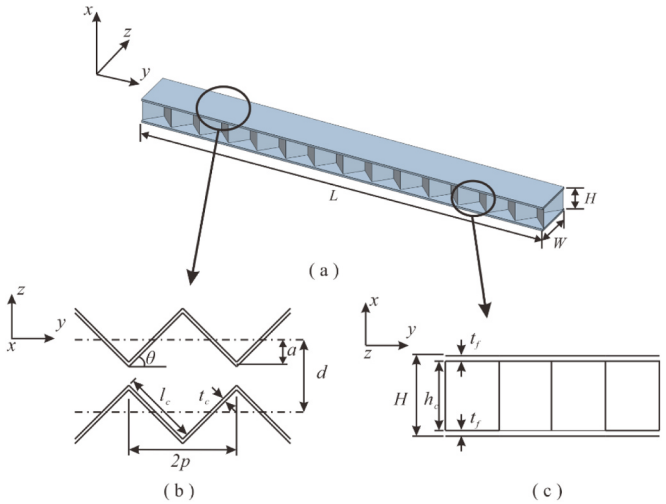

Fig. 2. (a) Schematic of sandwich beam with corrugated channel core, (b) top view and (c) lateral view.

fabrication methodology for Ti-6Al-4V sandwich panels with corrugated channel cores through stamping forming. However, stamping forming has two serious difficulties in fabricating corrugated channel cores at room temperature [34]. On one hand, it is hard to control the inclination angle of corrugated members due to high spring-back errors of Ti-6Al-4V sheets. On the other hand, stamping forming could result in cracks and even fracture on the side of connection nodes experiencing tensile stressing, due to the low ductility of Ti-6Al-4V. Queheillalt and Wadley [35] considered the relation between the minimum bend radius/sheet thickness ratio (the ratio at which cracks appear on the tensile stress side of nodes) and tensile elongations. Their experimental results indicated that the bend radius/sheet thickness ratio of Ti-6Al-4V should be kept in a range of 2.5–4. Nonetheless, these authors just attempted to avoid cracking during stamping forming process, and did not control the inclination angles of corrugated members. Rather, we adopted a modified fabrication method called the cutting forming method (CFM), which directly cut the needed core from a metal block. This fabrication technology not only avoids spring-back errors, but also controls precisely the inclination angle of corrugated members.

Both the corrugated channel core and the face sheets were all made of Ti-6Al-4V alloy, with $E = 126\,\text{GPa}$, $\nu = 0.34$ and $\rho = 4430\,\text{kg/m}^3$ [15]. The fabrication process of the sandwich beam shown in Fig. 3 is consisted of three main steps: (1) cutting the corrugated channel core through electro-discharge machining, (2) assembling the face sheets and the cores to form sandwich beam, and (3) vacuum brazing. Vacuum brazing was conducted in a furnace with a vacuum atmosphere of 5×10^{-3} Pa, using 40Ti-20Cu-20Ni-20Zr (wt%) braze alloy (Lucas Milhaupt Co., Ltd.) at 900 °C. The brazing temperature was preserved for 10 min [36] to let capillarity draw the brazing solder into the joints and the applied pressure came from a stainless steel weight [37], both leading to an excellent bond between the face sheets and the core. The test specimen contained 14 unit cells along the length direction, as shown in Fig. 5, with the following geometric parameters $L = 396\,\text{mm}$, $H = 24\,\text{mm}$, $W = 40\,\text{mm}$, $t_f = 2\,\text{mm}$, $t_c = 1\,\text{mm}$, $l_c = 20\,\text{mm}$, $h_c = 20\,\text{mm}$, $\theta = 45^\circ$ and $d = 20\,\text{mm}$.

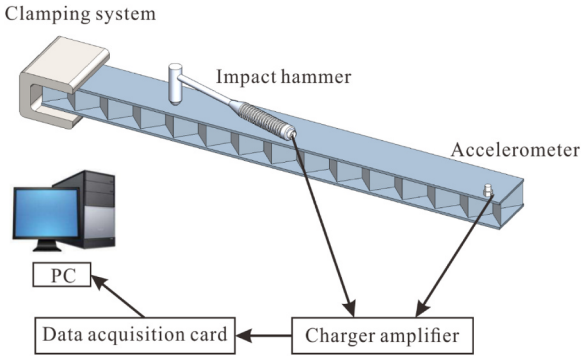

Fig. 4. The experimental system for modal analysis.

2.2. Experimental process

Modal test was performed on the fabricated sandwich beam under clamped-free boundary condition as shown in Fig. 4. In this test, the experimental system was comprised of an impact hammer (B&K), an accelerometer (KISTLER Type 8702B25M), a charge amplifier, a fixture and a modal analysis system (LMS Test Lab 14a). The charge amplifier was connected to a data acquisition card and PC. The modal analysis system installed on the PC was used to process the data. With point-by-point excitation method adopted, the sandwich beam was divided into 9 regions linked by 18 points (the impact points), as shown in Fig. 5.

We placed an accelerometer on point 1, and then applied an impact force by the impact hammer on points 1–18 in sequence. We used the piezoelectric sensor built in the impact hammer to generate the voltage signal, and then calibrated the electronically applied force signal. Generally, an accelerometer is consisted of a frame, a mass and a piezoelectric sensor. The excitation of impact hammer could vibrate the mass in the accelerometer and the built-in piezoelectric sensor generated the voltage signal. This voltage signal was calibrated using the response signals, including acceleration, velocity and displacement. The signals from the accelerometer (response signal) and the impact hammer (force signal) were transferred to a charge amplifier connected

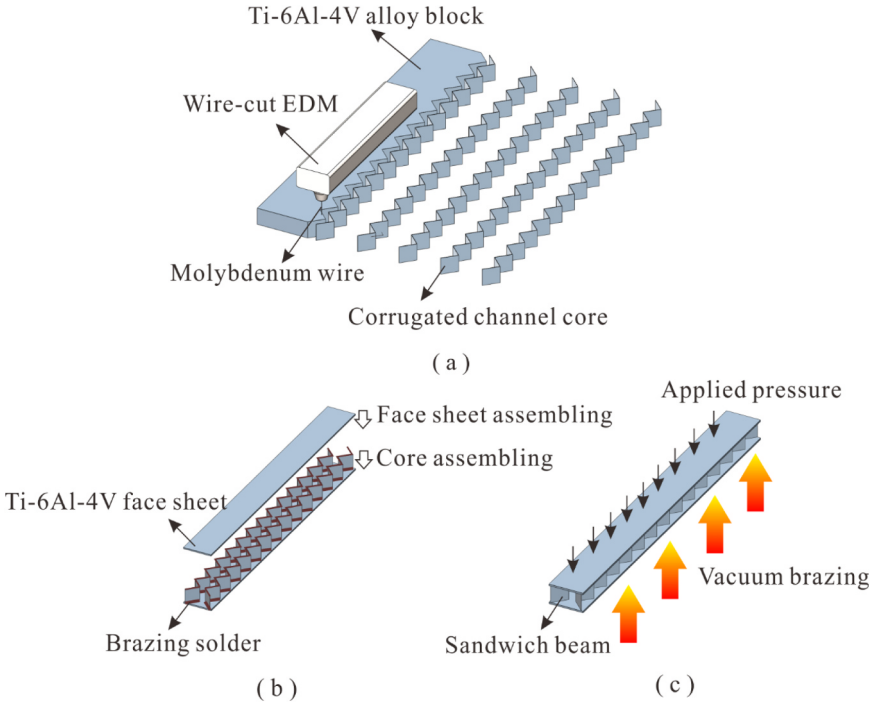

Fig. 3. Fabrication of sandwich beam with triangular corrugated channel core: (a) cutting the core; (b) assembling the sandwich beam; (c) vacuum brazing.

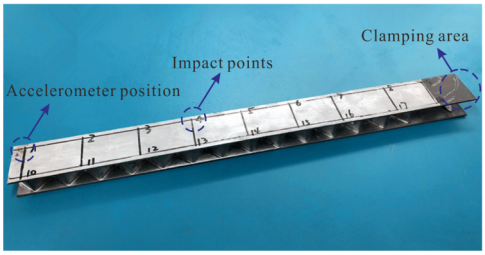

Fig. 5. Accelerometer position, impact points and clamping area for the sandwich beam.

to a data acquisition board and a PC. Based on the response and force signals, we used the modal analysis system (LMS Test Lab 14a) to calculate the frequency response function through Fast Fourier Transform (FFT) and then determine the natural frequencies and mode shapes.

Due to the special topology of corrugated channel core, the accelerometer was placed on the top of face sheet to measure the bending modes, but it could not be fixed on the core to measure the lateral modes. Therefore, the first two bending modes were experimentally measured and then compared with predictions of 2D and 3D numerical models. In contrast, the first two lateral modes were numerically calculated using both 2D and 3D models. In addition, the first torsional mode was also numerically simulated. For consistency, only average results from three experimental tests were reported below.

3. Finite element modeling

The vibration characteristics of sandwich beam with corrugated channel core were analyzed using FE simulations using both the equivalent FE model (2D model) and the three dimensional FE model (3D model). In the 2D model, the discrete corrugated channel core was treated as an equivalent homogeneous core. The corresponding effective stiffness matrix C^Hcould be obtained using the homogenization method, as (details given in the Appendix A):

$$C^H = \begin{bmatrix} C_{11}^H & C_{12}^H & C_{13}^H & 0 & 0 & 0 \\ & C_{22}^H & C_{23}^H & 0 & 0 & 0 \\ sym & & C_{33}^H & 0 & 0 & 0 \\ 0 & 0 & 0 & C_{44}^H & 0 & 0 \\ 0 & 0 & 0 & 0 & C_{55}^H & 0 \\ 0 & 0 & 0 & 0 & 0 & C_{66}^H \end{bmatrix} \tag{2}$$

where

$$C_{11}^H = \bar{\rho}\frac{E}{1-\nu^2} \tag{3}$$

$$C_{22}^H = \frac{2a}{d}\left[\frac{E}{1-\nu^2}\left(\frac{t_c}{l_c}\right)\frac{\cos^3\theta}{\sin\theta} + \frac{E}{1-\nu^2}\left(\frac{t_c}{l_c}\right)^3 \sin\theta\cos\theta\right] \tag{4}$$

$$C_{33}^H = \frac{2a}{d}\left[\frac{E}{1-\nu^2}\left(\frac{t_c}{l_c}\right)\frac{\sin^3\theta}{\cos\theta} + \frac{E}{1-\nu^2}\left(\frac{t_c}{l_c}\right)^3 \sin\theta\cos\theta\right] \tag{5}$$

$$C_{23}^H = \frac{2a}{d}\left[\frac{E}{1-\nu^2}\left(\frac{t_c}{l_c}\right)\sin\theta\cos\theta - \frac{E}{1-\nu^2}\left(\frac{t_c}{l_c}\right)^3 \sin\theta\cos\theta\right] \tag{6}$$

$$C_{44}^H = \frac{2a}{d}\left[\frac{E}{1-\nu^2}\left(\frac{t_c}{l_c}\right)\sin\theta\cos\theta + \frac{1}{4}\frac{E}{1-\nu^2}\left(\frac{t_c}{l_c}\right)^3 \times\left(\frac{\sin^3\theta}{\cos\theta} + \frac{\cos^3\theta}{\sin\theta} - 2\sin\theta\cos\theta\right)\right] \tag{7}$$

$$C_{12}^H = \bar{\rho}\frac{\nu E}{1-\nu^2}\frac{\cos\theta}{\sin\theta} \tag{8}$$

$$C_{13}^H = \bar{\rho}\frac{\mu E}{1-\mu^2}\frac{\sin\theta}{\cos\theta} \tag{9}$$

$$C_{55}^H = \bar{\rho}G\sin^2\theta \tag{10}$$

$$C_{66}^H = \bar{\rho}G\sin^2\theta \tag{11}$$

The commercial finite element code ABAQUS v6.14 (Hibbitt, Karlsson & Sorensen, Inc.) was employed to obtain the natural frequencies and mode shapes of the sandwich beam. In the 3D model, the corrugated channel core was meshed using linear quadrilateral shell elements with induced integration (S4R) and the face sheets were discretized using eight-node linear brick elements with reduced integration (C3D8R). In the 2D model, C3D8Rs were used to mesh both the equivalent core and the face sheets. A mesh sensitivity study was carried out to ensure convergence of the numerical results. Subsequently, a linear perturbation analysis step was created, and the frequency extraction procedure was carried out with the subspace solver. The maximum number of iterations was set at 100. In the FE models, the corrugated channel core and the face sheets were tied together. On one end of the sandwich beam, all degrees of freedom including displacements and rotations were restrained.

4. Results and discussion

4.1. Validation study

The first two bending modes (natural frequencies and mode shapes) of the sandwich beam with corrugated channel core were obtained using the 2D model, the 3D model and the experimental tests, as shown in Fig. 6 and Table 1. It is seen that results obtained from the 2D model agreed well with those from the 3D model and experiments. The mode shapes obtained from the three different methods were the same. The first two bending natural frequencies (f_1 and f_3) predicted by the 2D model were very close to those of the 3D model, with an error was less than 1%. The experimental results were relatively lower than those of the 2D and 3D models. The discrepancy might be caused by (1) the damping effect, (2) the additional mass of the brazing solder and accelerometer, and (3) the experimental boundary condition (weaker than clamped boundary condition assumed in FE simulations).

In addition to natural frequency, the first two lateral modes were also investigated using 2D and 3D FE models and the results are displayed in Fig. 7 and Table 2. As shown in Table 2, the error between the two FE models was less than 1%. In addition, Fig. 8 compares the mode shapes of the first torsional mode calculated by the 3D model with those by the 2D model. Correspondingly, the natural frequency of the first torsional mode was 954.20 Hz by the 3D model, relative to 1016.40 Hz by the 2D model, approximately 6.5% higher than the former. Similar results were reported in several prior studies [13,14,38].

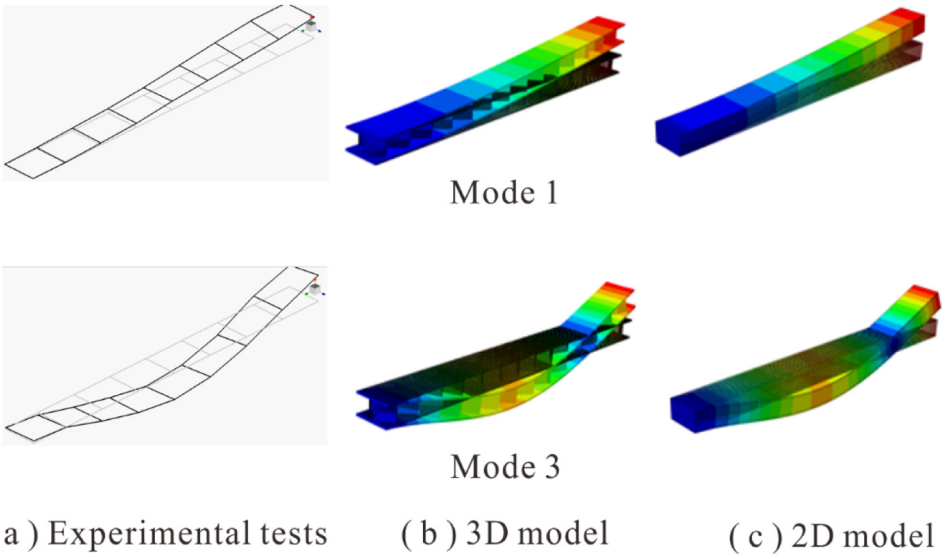

Fig. 6. The first two bending mode shapes obtained from (a) experimental test, (b) 3D FE model and (c) 2D FE model.

Table 1
The first two bending natural frequencies (Hz) obtained using three different methods.

Order	3D FE model	2D FE model	Experimental test
f_1 (1st bending mode)	176.37	176.87	166.28
f_3(2nd bending mode)	962.12	981.07	912.25

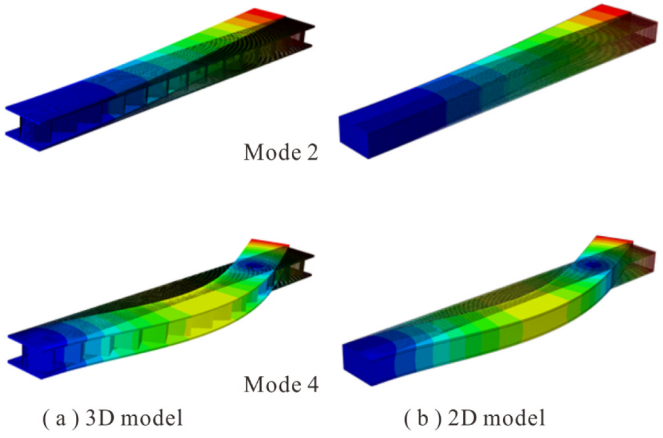

Fig. 7. The first two lateral mode shapes predicted by (a) 3D model and (b) 2D model.

Table 2
The first two lateral natural frequencies (Hz) predicted by 2D and 3D FE models.

Order	3D model	2D model
f_2 (1st lateral mode)	188.33	188.53
f_4 (2nd lateral mode)	1129.4	1135.6

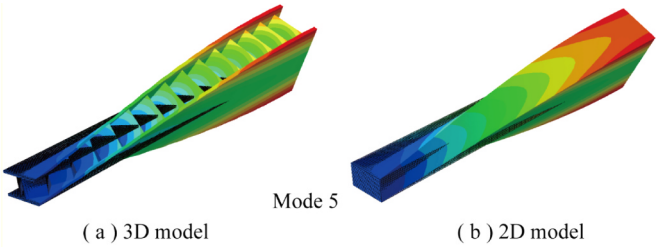

Fig. 8. The first torsional mode shapes predicted from (a) 3D model and (b) 2D model.

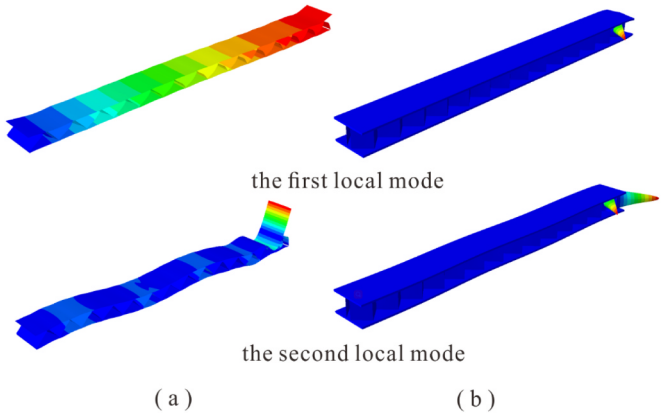

Fig. 9. The first two local mode shapes of sandwich beam cored with (a) corrugations and (b) corrugated channels.

4.2. Enhancement achieved by the proposed core topology

In terms of local vibration modes and anisotropy of the sandwich core, a comparative analysis was carried out between the traditional corrugated core and the present corrugated channel core. The vibration properties of the corrugated-core sandwich beam having the same mass

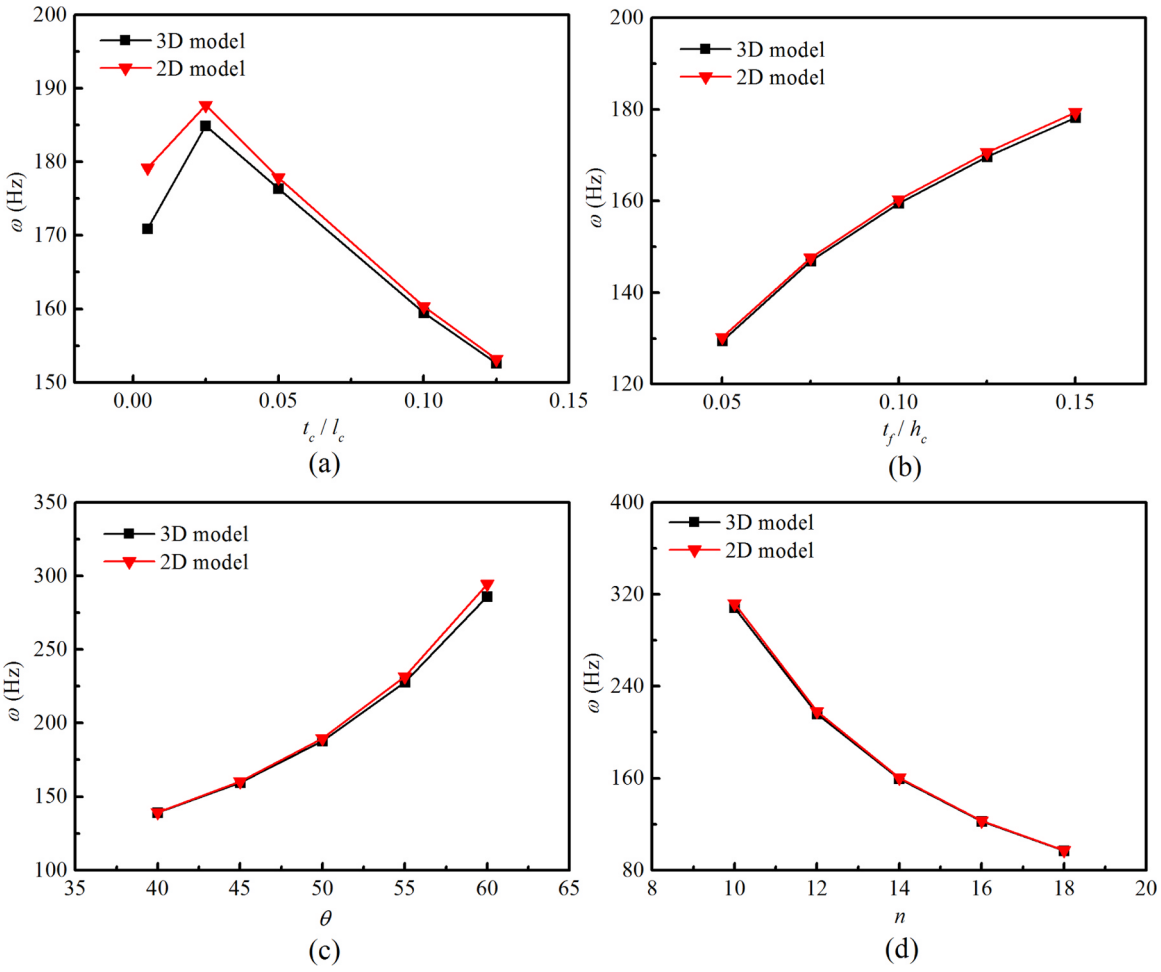

Fig. 10. Effects of geometric parameters on the first natural frequency of sandwich beam: (a) slenderness ratio of corrugated member t_c/l_c; (b) face sheet thickness ratio t_f/h_c; (c) inclination angle of corrugated member θ; (d) number of unit cells n.

as that given in Section 4.1 were also calculated using ABAQUS. As shown in Fig. 9**(a)**, the first two local modes appeared as the seventh and eleventh modes and the corresponding natural frequencies were 2906.5 Hz and 4939.4 Hz. In comparison, the first two local vibration modes of the current sandwich beam started as the sixteenth and seventeenth modes as shown in Fig. 9**(b)** and the natural frequencies were 6809.2 Hz and 6918.6 Hz, respectively. The results revealed that the corrugated channel core leads to significantly suppressed local vibration modes.

Besides, according to Liu et al. [38], the effective shear stiffness of a corrugated core along its transverse and longitudinal directions were different, thus causing the anisotropy of sandwich beams in three-point bending [10] and dynamic impacting [12]. In Section 4.1, the effective elastic properties of corrugated channel cores obtained via homogenization were validated. For the present core topology, the effective shear moduli along the transverse and longitudinal directions were the same (Appendix A). Therefore, the anisotropy of the proposed core topology is not as significant as the corrugated core.

4.3. Effects of geometric parameters

The effects of relevant geometrical parameters such as the slenderness ratio t_c/l_c, the face sheet thickness ratio t_f/h_c, the inclination angle of corrugated member θ and the number of unit cells n on the first natural frequency quantified using 2D and 3D FE models.

To highlight the superiority of sandwich beams over solid beams, a dimensionless natural frequency parameter is proposed as ω/ω_0, where ω and ω_0 are the first natural frequency of the sandwich beam and the corresponding solid beam having the same length, width, weight and boundary conditions, respectively. The height of the solid beam can be obtained as:

$$h = \bar{\rho} h_c + 2t_f \tag{12}$$

Thus, based on the theory of Bernoulli-Euler beams, the first natural frequency of the solid beam is given by [13,27]:

$$\omega_0 = \frac{1.01}{2\pi}\sqrt{\frac{Eh^2}{\rho L^4}} \tag{13}$$

where ρ and E are the density and Young's modulus of the base material, and L is the length of the solid beam.

Fig. 10 presents the effects of geometric parameters on the first natural frequency. As the slenderness ratio t_c/l_c grows, the natural frequency firstly increases and then decreases. Obviously, a higher t_c/l_c leads to a higher structural stiffness and a larger weight, although the ratio of structural stiffness and weight may not increase. The effects of face sheet thickness ratio t_f/h_c and corrugation angle θ are consistent. It

Table 3
Effects of geometric parameters on natural frequency: comparison between sandwich beam and the corresponding solid beam.

Varied geometrical parameter	Sandwich beam		Solid beam	
	3D model (Hz)	2D model (Hz)	Error (%)	Hz
Slenderness ratio t_c/l_c				
0.005	170.93	179.18	4.83	22.64
0.025	184.92	187.69	1.50	25.74
0.05	176.37	176.87	0.28	29.60
0.1	159.5	160.35	0.53	37.33
0.125	152.62	153.17	0.36	41.20
Face sheet thickness t_f/h_c				
0.05	129.47	130.26	0.61	26.40
0.075	146.92	147.6	0.46	31.87
0.1	159.5	160.35	0.53	37.33
0.125	169.68	170.63	0.56	42.80
0.15	178.2	179.37	0.66	48.27
Inclination angle of corrugation θ				
40	139.12	139.3	0.13	30.80
45	159.5	160.35	0.53	37.33
50	187.81	189.6	0.95	47.05
55	227.77	231.61	1.69	62.21
60	286.13	294.48	2.92	87.48
Number of unit cells n				
10	308.33	312.03	1.20	73.17
12	215.98	218.21	1.03	50.82
14	159.5	160.35	0.53	37.33
16	122.52	122.98	0.38	28.58
18	97.03	97.28	0.26	22.58

is observed that as t_f/h_c or θ is increased, the natural frequency increases. Concerning the number of unit cells n, it was found that it plays an important role in the computational accuracy of 2D FE simulations. When n increases, the equivalent core constituted by the discrete unit cells increasingly approaches the corresponding continuous core, reducing thus the computational error. Table 3 displays the first natural frequencies predicted with 2D and 3D models for selected geometric parameters.

Fig. 11 shows the superiority of the proposed sandwich beam over the solid beam. The effects of slenderness ratio t_c/l_c, face sheet thickness ratio t_f/h_c and angle of corrugated member θ are consistent. It is noted that as t_c/l_c, t_f/h_c or θ is increased, the superiority of the sandwich beam gets weaker. Among the three geometric parameters, the effects of t_c/l_c on the dimensionless natural frequency are greater. Besides, when the number of unit cells n increases, the superiority of sandwich beam remains nearly constant.

4.4. Comparison with competing cores

A number of theoretical models have been developed to characterize the vibration properties of sandwich beams, such as the Allen model [39], the equivalent single layer (ESL) model [40,41], the layer wise (LW) model [42,43] and the zig-zag (ZZ) model [44,45]. These models substantiated a common belief that the first natural frequency of the sandwich beam is determined by its flexural rigidity and transverse shear stiffness. Based on the first shear deformation theory, Timoshenko [46,47] gave an analytical solution to the natural frequency p_m of prismatic beams with simple supported ends, as:

$$p_m = \frac{\pi^2}{L^2}\sqrt{\frac{EIg}{\rho\Omega}}\left[1 - \frac{1}{2}\frac{\pi^2 I}{L^2\Omega}\left(1 + \frac{E}{\lambda\Lambda}\right)\right] \tag{14}$$

where Λ is the modulus of transverse shear stiffness, λ is a constant relying upon the shape of the cross-section, L is the length of a wave, EI is the flexural rigidity of the prismatic bar, Ω is the area of the cross-section, and ρ/g is the density of the base material. As shown in **Eq.** (14), as the transverse shear modulus is increased, the natural frequency increases. In terms of flexural rigidity, for a sandwich beam, the part contributed by the face sheets is dominant and the part contributed by the core can be ignored so that the core mainly dedicates the transverse shear stiffness of the sandwich beam [39]. When the face sheets are the same, the transverse shear stiffness of the core governs the first natural frequency of the sandwich beam. Based on the homogenization method, the effective transverse shear stiffness of the corrugated channel core is compared with competing core topologies (tetrahedral, Kagome and pyramidal trusses; hexagonal honeycombs), as shown in Fig. 12 and listed as follows [32,48,49]:

Tetrahedral or Kagome truss: $C_{tetrahedral} = C_{Kagome} = \frac{1}{9}\bar{\rho}E$ (15)

Pyramidal truss: $C_{pyramid} = \frac{1}{8}\bar{\rho}E$ (16)

Hexagonal honeycomb: $C_{hexagonal} = \frac{1}{2}\bar{\rho}G$ (17)

Corrugated channel core: $C_{corrugated} = \bar{\rho}G\sin^2\theta$ (18)

As the Poisson ratio varies in a range of $0 < \nu < 0.5$, the effective transverse shear stiffness of the corrugated channel core lies within the range:

$$\frac{1}{3}\bar{\rho}E\sin^2\theta < C_{corrugated} = \bar{\rho}G\sin^2\theta < \frac{1}{2}\bar{\rho}E\sin^2\theta \tag{19}$$

According to **Eq.** (18), the inclination angle θ has direct effect on the effective transverse shear stiffness. When $\theta > 20.7^\circ$, the effective transverse shear stiffness of the corrugated channel core is higher than that of tetrahedral, Kagome or pyramidal truss core. When $\theta > 45^\circ$, it is even higher than that of hexagonal honeycomb.

5. Concluding remarks

Sandwich beams with corrugated channel cores are particularly attractive for multi-functional applications. Their vibration properties (natural frequencies and mode shapes) are investigated through experiments and FE simulations. FE simulations with both 2D and 3D models are used to calculate the natural frequencies and capture the mode shapes. The main findings of the present study are:

(1) The effective elastic properties of the corrugated channel cores calculated using the homogenization method can be employed to predict accurately the global vibration properties, as validated by experimental data and full 3D FE simulations.
(2) Compared to traditional corrugated core, the proposed corrugated channel core for sandwich construction can suppress local vibration modes and weaken the anisotropy of the sandwich.
(3) When the inclination angle of corrugated member exceeds 45°, the first natural frequency of sandwich beams with corrugated channel cores is higher than those of competing core topologies (tetrahedral, Kagome and pyramidal trusses and hexagonal honeycombs).
(4) The first natural frequency of the proposed sandwich beam is higher than that of solid beam having the same mass.

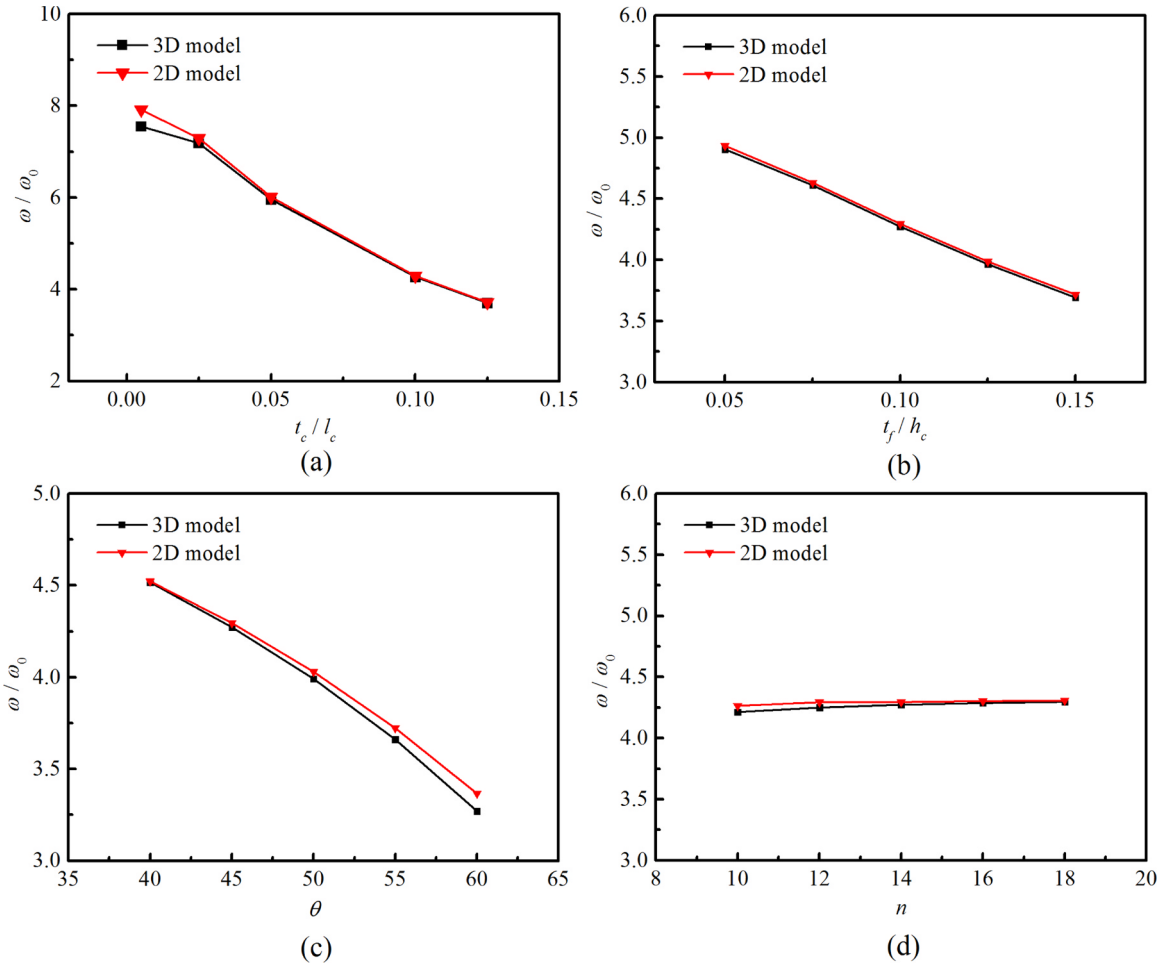

Fig. 11. Effects of geometric parameters on dimensionless frequency parameter of sandwich beam: (a) slenderness ratio of corrugated member t_c/l_c; (b) face sheet thickness ratio t_f/h_c; (c) inclination angle of corrugated member θ; (d) number of unit cells n.

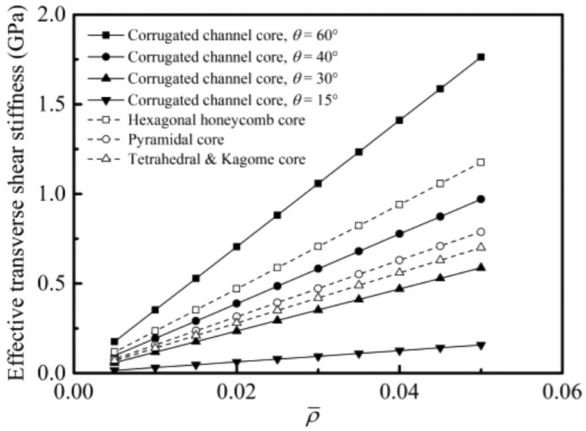

Fig. 12. Effect of core topology on effective transverse shear stiffness (base material: Ti-6Al-4V).

This work ushers in designing more complex sandwich structures (plates and shells) with corrugated channel cores and contributes as further fundamental research on applications of these novel sandwich structures, such as the pulse detonation engines.

Acknowledgments

This work was supported by the National Key Research and Development Program of China (2017YFB1102801), the Open Project for Key Laboratory of Intense Dynamic Loading and Effect (KLIDLE1801), National Natural Science Foundation of China (11472209 and 11472208), China Postdoctoral Science Foundation (2016M600782), Zhejiang Provincial Natural Science Foundation of China (LGG18A020001), Postdoctoral Scientific Research Project of Shaanxi Province (2016BSHYDZZ18).

Appendix A

For a unit cell of the corrugated channel core, the effective elastic stiffness matrix is derived in the spirit of Liu et al. [50]. Similar to the homogenization framework of honeycombs [32] and 2D corrugated cores [38], the unit cell is discretized into Euler-Bernoulli beam units. The strain energy density of the corrugated channel core can thence be written as:

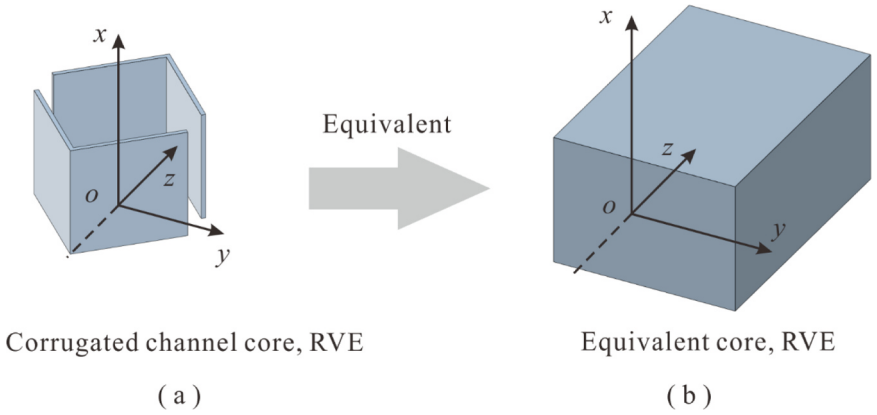

Fig. A1. Representative volume element (RVE or unit cell) of (a) corrugated channel core and (b) equivalent core.

$$\bar{U} = \frac{1}{V}\sum_{1}^{n}\frac{1}{2}\tilde{\mathrm{u}}^{(i)T}\tilde{\mathrm{K}}^{(i)T}\tilde{\mathrm{u}}^{(i)} \tag{A1}$$

where $\tilde{\mathrm{u}}^{(i)}$ is the global nodal displacement vector for the *i*th beam unit, and $\tilde{\mathrm{K}}^{(i)}$ is the global stiffness matrix of the *i*th beam unit. Note that, Liu et al. [50] investigated the calculation accuracy of Euler-Bernoulli beam unit and found that Timoshenko beam unit hardly improves the calculation accuracy of thin sandwich structures. As shown in Fig. A1, the unit cell of the corrugated channel core contains four beam units ($n = 4$).

Here, we consider the deformation of a beam unit subjected to a $\bar{y} - \bar{z}$ plane macroscopic strain E as schematically shown in Fig. A2**(a)**. According to prior research [15], it is assumed that the beam unit is clamped at both ends. $\tilde{\mathrm{u}}^{(i)}$ is the global nodal displacement vector characterized by end nodes α and β in Fig. A2 **(b)** and can be described as:

$$\tilde{\mathrm{u}}^{(i)} = \mathrm{T}^{T}\tilde{\mathrm{u}}^{(i)e} \tag{A2}$$

$$\tilde{\mathrm{u}}^{(i)e} = (w_\alpha \quad v_\alpha \quad \theta_\alpha \quad w_\beta \quad v_\beta \quad \theta_\beta) \tag{A3}$$

$$\mathrm{T} = \begin{bmatrix} \cos\theta & \sin\theta & 0 & 0 & 0 & 0 \\ -\sin\theta & \cos\theta & 0 & 0 & 0 & 0 \\ 0 & 0 & 1 & 0 & 0 & 0 \\ 0 & 0 & 0 & \cos\theta & \sin\theta & 0 \\ 0 & 0 & 0 & -\sin\theta & \cos\theta & 0 \\ 0 & 0 & 0 & 0 & 0 & 1 \end{bmatrix} \tag{A4}$$

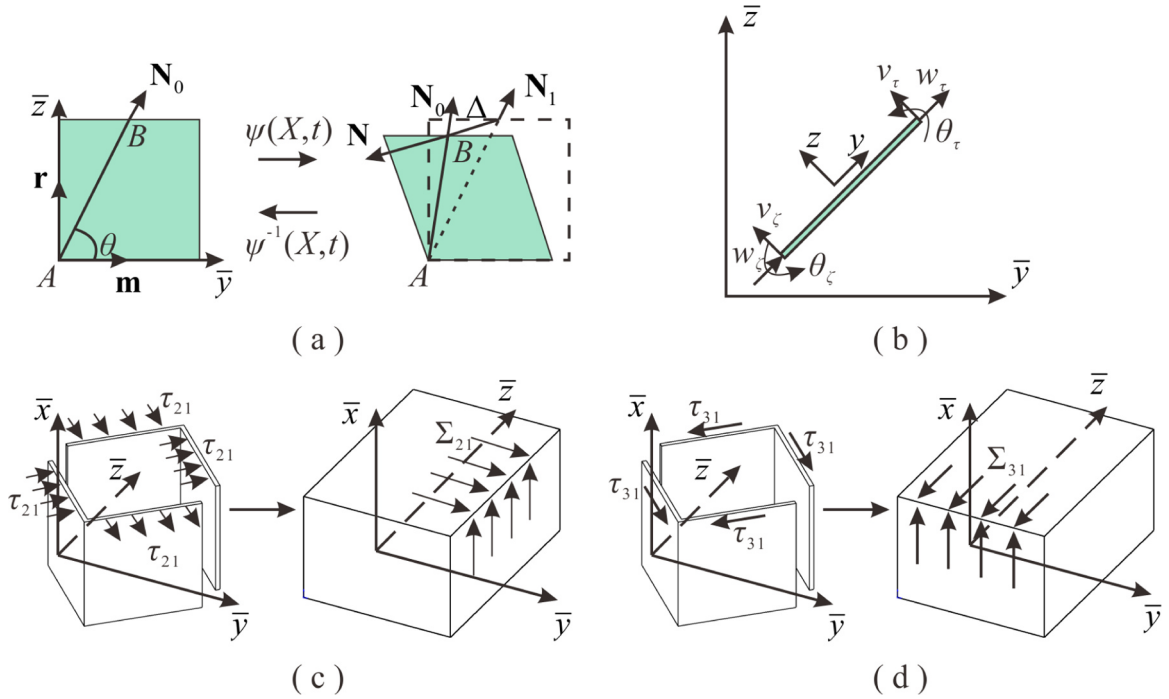

Fig. A2. Homogenization of corrugated channel core: (a) the kinematics of an inclined corrugated member; (b) an inclined corrugated member subjected to nodal forces/moments; (c) shear flow in a typical cell and its representative volume element when: (c) macroscopic shear stress τ_{21} or (d) macroscopic shear stress τ_{31} is imposed.

where $\tilde{u}^{(i)e}$ denotes the nodal displacement vector in under local coordinates (y, z), **T** is the transformation matrix between local and global coordinates, superscript e represents values in local coordinates and superscript T represents the transpose of a matrix. The global nodal displacement vector for the ith beam can be written as:

$$\tilde{u}^{(i)} = (\Delta_1 \quad \Delta_2 \quad 0 \quad 0 \quad 0 \quad 0)^{(i)T} \tag{A5}$$

where Δ_1 and Δ_2 denote the projections of end node displacement Δ, given by:

$$\Delta = \frac{2a}{\sin\theta} E \mathrm{N}_0 \tag{A6}$$

where

$$\mathrm{N}_0 = (\cos\theta,\ \sin\theta)^T,\ \mathrm{E} = \begin{bmatrix} E_{22} & E_{23} \\ sym & E_{33} \end{bmatrix},\ \Delta = (\Delta_1 \mathrm{m} \quad \Delta_2 \mathrm{r})^T \tag{A7}$$

$\mathbf{N_0}$ denotes the unit vector along which the inclined beam is initially aligned and the volume of the current unit cell $\Omega = 4pd$. $\tilde{K}^{(i)}$is the global stiffness matrix that satisfies the transformation between local and global coordinates as shown in Fig. A2**(b)**:

$$\tilde{K}^{(i)} = T^T \tilde{K}^{(i)e} T \tag{A8}$$

$$\tilde{K}^{(i)e} = \begin{bmatrix} \frac{EA}{l} & 0 & 0 & -\frac{EA}{l} & 0 & 0 \\ 0 & \frac{12EI}{l^3} & \frac{6EI}{l^2} & 0 & -\frac{12EI}{l^3} & \frac{6EI}{l^2} \\ 0 & \frac{6EI}{l^2} & \frac{4EI}{l} & 0 & -\frac{6EI}{l^2} & \frac{2EI}{l} \\ -\frac{EA}{l} & 0 & 0 & \frac{EA}{l} & 0 & 0 \\ 0 & -\frac{12EI}{l^3} & -\frac{6EI}{l^2} & 0 & \frac{12EI}{l^3} & -\frac{6EI}{l^2} \\ 0 & \frac{6EI}{l^2} & \frac{2EI}{l} & 0 & -\frac{6EI}{l^2} & \frac{4EI}{l} \end{bmatrix} \tag{A9}$$

where $\tilde{K}^{(i)e}$ is the local stiffness matrix of the i-th beam.

For linear elastic medium, the stress-strain relation can be obtained by

$$C^H_{ijkl} = \frac{\partial^2 U_0^*}{\partial \varepsilon^*_{ij} \partial \varepsilon^*_{kl}} \tag{A10}$$

The $\bar{y} - \bar{z}$ plane macroscopic effective stiffness of the corrugated channel core can be written as:

$$C^H_{22} = \frac{2a}{d}\left[\frac{E}{1-\nu^2}\left(\frac{t_c}{l_c}\right)\frac{\cos^3\theta}{\sin\theta} + \frac{E}{1-\nu^2}\left(\frac{t_c}{l_c}\right)^3 \sin\theta\cos\theta\right] \tag{A11}$$

$$C^H_{33} = \frac{2a}{d}\left[\frac{E}{1-\nu^2}\left(\frac{t_c}{l_c}\right)\frac{\sin^3\theta}{\cos\theta} + \frac{E}{1-\nu^2}\left(\frac{t_c}{l_c}\right)^3 \sin\theta\cos\theta\right] \tag{A12}$$

$$C^H_{23} = \frac{2a}{d}\left[\frac{E}{1-\nu^2}\left(\frac{t_c}{l_c}\right)\sin\theta\cos\theta - \frac{E}{1-\nu^2}\left(\frac{t_c}{l_c}\right)^3 \sin\theta\cos\theta\right] \tag{A13}$$

$$C^H_{44} = \frac{2a}{d}\left[\frac{E}{1-\nu^2}\left(\frac{t_c}{l_c}\right)\sin\theta\cos\theta + \frac{1}{4}\frac{E}{1-\nu^2}\left(\frac{t_c}{l_c}\right)^3 \times \left(\frac{\sin^3\theta}{\cos\theta} + \frac{\cos^3\theta}{\sin\theta} - 2\sin\theta\cos\theta\right)\right] \tag{A14}$$

If a macroscopic strain E_{11} is solely imposed on the core, the local normal stress σ^c_x in the $\bar{x}-$ direction is given by:

$$\sigma^c_x = \frac{E}{1-\nu^2} E_{11} \tag{A15}$$

It follows that the macroscopic stress is

$$\sigma_x = \bar{\rho}\sigma^c_x \tag{A16}$$

so that

$$C^H_{11} = \bar{\rho}\frac{E}{1-\nu^2} \tag{A17}$$

If E_{22} or E_{33} is solely imposed on the core, the macroscopic stress can be obtained by using nodal displacements and the corresponding equilibrium equations. Consequently, C^H_{12} and C^H_{13} can be written as:

$$C^H_{12} = \bar{\rho}\frac{\nu E}{1-\nu^2}\frac{\cos\theta}{\sin\theta} \tag{A18}$$

$$C^H_{13} = \bar{\rho}\frac{\nu E}{1-\nu^2}\frac{\sin\theta}{\cos\theta} \tag{A19}$$

When subjected to a macroscopic shear strain E_{21} or E_{31}, the resulting distributed shear flow in a unit cell is shown in Fig. A2**(c)** and **(d)**. The

corresponding equilibrium equations can be written as:

$$\sum_{21} \Omega = 2\tau_{21} t_c l_c \sin\theta \tag{A20}$$

$$\sum_{31} \Omega = 2\tau_{31} t_c l_c \sin\theta \tag{A21}$$

In both cases, due to symmetric layout of the unit cell, all inclined core members have the same local out-of-plane shear stresses, τ_{21} and τ_{31}. The local shear strains can be written accordingly, as:

$$\varepsilon_{21} = \frac{\tau_{21}}{2G} \tag{A22}$$

$$\varepsilon_{31} = \frac{\tau_{31}}{2G} \tag{A23}$$

Using the micro-macro relationship [51], we have:

$$\frac{1}{2} C_{66}^{H} (2E_{21})^2 \Omega = \frac{1}{2} G \left(\frac{\tau_{21}}{G}\right)^2 t_c l_c \tag{A24}$$

$$\frac{1}{2} C_{55}^{H} (2E_{31})^2 \Omega = \frac{1}{2} G \left(\frac{\tau_{31}}{G}\right)^2 t_c l_c \tag{A25}$$

from which:

$$C_{55}^{H} = \bar{\rho} G \sin^2\theta \tag{A26}$$

$$C_{66}^{H} = \bar{\rho} G \sin^2\theta \tag{A27}$$

References

[1] T.J. Lu, H.A. Stone, M.F. Ashby, Heat transfer in open-cell metal foams, Acta Mater. 46 (1998) 3619–3635.
[2] T.J. Lu, Heat transfer efficiency of metal honeycombs, Int. J. Heat Mass Transf. 42 (1999) 2031–2040.
[3] T.J. Lu, L. Valdevit, A.G. Evans, Active cooling by metallic sandwich structures with periodic cores, Prog. Mater. Sci. 50 (2005) 789–815.
[4] L.L. Yan, B. Yu, B. Han, C.Q. Chen, Q.C. Zhang, T.J. Lu, Compressive strength and energy absorption of sandwich panels with aluminum foam-filled corrugated cores, Compos. Sci. Technol. 86 (2013) 142–148.
[5] M.F. Ashby, T.J. Lu, Metal foams: a survey, Sci. China Ser. B - Chem. 46 (2003) 521–532.
[6] W. Jiang, L. Yan, H. Ma, Y. Fan, J. Wang, M. Feng, S. Qu, Electromagnetic wave absorption and compressive behavior of a three-dimensional metamaterial absorber based on 3D printed honeycomb, Sci. Rep. 8 (2018) 4817.
[7] T.J. Lu, A. Hess, M.F. Ashby, Sound absorption in metallic foams, J. Appl. Phys. 85 (1999) 7528–7539.
[8] T.J. Lu, F. Chen, D.P. He, Sound absorption of cellular metals with semiopen cells, J. Acoust. Soc. Am. 108 (2000) 1697–1709.
[9] C. Shen, Q.C. Zhang, S.Q. Chen, H.Y. Xia, F. Jin, Sound transmission loss of adhesively bonded sandwich panels with pyramidal truss core: theory and experiment, Int. J. Appl. Mech. 7 (2015) 16.
[10] L. Valdevit, J.W. Hutchinson, A.G. Evans, Structurally optimized sandwich panels with prismatic cores, Int. J. Solids Struct. 41 (2004) 5105–5124.
[11] L. Valdevit, N. Vermaak, F.W. Zok, A.G. Evans, A materials selection protocol for lightweight actively cooled panels, J. Appl. Mech. 75 (2008) 061022.
[12] V. Rubino, V.S. Deshpande, N.A. Fleck, The dynamic response of end-clamped sandwich beams with a Y-frame or corrugated core, Int. J. Impact Eng. 35 (2008) 829–844.
[13] Z.J. Zhang, B. Han, Q.C. Zhang, F. Jin, Free vibration analysis of sandwich beams with honeycomb-corrugation hybrid cores, Compos. Struct. 171 (2017) 335–344.
[14] B. Han, K.K. Qin, Q.C. Zhang, Q. Zhang, T.J. Lu, B.H. Lu, Free vibration and buckling of foam-filled composite corrugated sandwich plates under thermal loading, Compos. Struct. 172 (2017) 173–189.
[15] Z.Y. Zhao, B. Han, X. Wang, Q.C. Zhang, T.J. Lu, Out-of-plane compression of Ti-6Al-4V sandwich panels with corrugated channel cores, Mater. Des. 137 (2018) 463–472.
[16] M. Mirzaei, M.J. Torkaman Asadi, R. Akbari, On vibrational behavior of pulse detonation engine tubes, Aerosp. Sci. Technol. 47 (2015) 177–190.
[17] L. Tian, L.H. Chen, Q. Chen, F.Q. Zhong, X.Y. Chang, Engine performance analysis and optimization of a dual-mode scramjet with varied inlet conditions, Acta Mech. Sin. 32 (2015) 75–82.
[18] X. Xue, Y. Yu, Q. Zhang, Study on the influences of interaction behaviors between multiple combustion-gas jets on expansion characteristics of Taylor cavities, Acta Mech. Sin. 31 (2015) 720–731.
[19] K. Matsuoka, K. Muto, J. Kasahara, H. Watanabe, A. Matsuo, T. Endo, Investigation of fluid motion in valveless pulse detonation combustor with high-frequency operation, P. Combust. Inst. 36 (2017) 2641–2647.
[20] W. Fan, C. Yan, X. Huang, Q. Zhang, L. Zheng, Experimental investigation on two-phase pulse detonation engine, Combust. Flame 133 (2003) 441–450.
[21] J.M. Kim, H.S. Han, J.Y. Choi, The experimental study about the effect of operating conditions on multi-tube pulse detonation engine performance, Int. J. Aeronaut. Space Sci. 19 (2018) 89–99.
[22] A.S. Sayyad, Y.M. Ghugal, Bending, buckling and free vibration of laminated composite and sandwich beams: a critical review of literature, Compos. Struct. 171 (2017) 486–504.
[23] P.R. Heyliger, J.N. Reddy, A higher-order beam finite-element for bending and vibration problems, J. Sound Vib. 126 (1988) 309–326.
[24] P. Subramanian, Dynamic analysis of laminated composite beams using higher order theories and finite elements, Compos. Struct. 73 (2006) 342–353.
[25] J. Lou, L. Ma, L.Z. Wu, Free vibration analysis of simply supported sandwich beams with lattice truss core, Mater. Sci. Eng. B 177 (2012) 1712–1716.
[26] J. Lou, L.Z. Wu, L. Ma, J. Xiong, B. Wang, Effects of local damage on vibration characteristics of composite pyramidal truss core sandwich structure, Compos. Part B - Eng. 62 (2014) 73–87.
[27] A. Boudjemai, R. Amri, A. Mankour, H. Salem, M.H. Bouanane, D. Boutchicha, Modal analysis and testing of hexagonal honeycomb plates used for satellite structural design, Mater. Des. 35 (2012) 266–275.
[28] S. Zghal, R. Nasri, Experimental investigation for forced vibration of honeycomb sandwich beams, Adv. Acoust. Vib. 5 (2017) 223–233.
[29] J. Yang, J. Xiong, L. Ma, G. Zhang, X. Wang, L. Wu, Study on vibration damping of composite sandwich cylindrical shell with pyramidal truss-like cores, Compos. Struct. 117 (2014) 362–372.
[30] Z. Zhao, S. Wen, F. Li, Vibration analysis of multi-span lattice sandwich beams using the assumed mode method, Compos. Struct. 185 (2018) 716–727.
[31] A.A. Khdeir, O.J. Aldraihem, Free vibration of sandwich beams with soft core, Compos. Struct. 154 (2016) 179–189.
[32] Jr Hohe, W. Becker, Effective stress-strain relations for two-dimensional cellular sandwich cores: homogenization, material models, and properties, Appl. Mech. Rev. 55 (2002) 61.
[33] T. Liu, Z.C. Deng, T.J. Lu, Design optimization of truss-cored sandwiches with homogenization, Int. J. Solids Struct. 43 (2006) 7891–7918.
[34] O.M. Badr, B. Rolfe, P. Hodgson, M. Weiss, Forming of high strength titanium sheet at room temperature, Mater. Des. 66 (2015) 618–626.
[35] D.T. Queheillalt, H.N.G. Wadley, Titanium alloy lattice truss structures, Mater. Des. 30 (2009) 1966–1975.
[36] T. Onzawa, A. Suzumura, M.W. Ko, Brazing of Titanium using low-melting-point Ti-based filler metals, Weld. J. 69 (1990) S462–S467.
[37] J. Cao, Z.J. Zheng, L.Z. Wu, J.L. Qi, Z.P. Wang, J.C. Feng, Processing, microstructure and mechanical properties of vacuum-brazed Al_2O_3/Ti6Al4V joints, Mater. Sci. Eng. A 535 (2012) 62–67.
[38] T. Liu, Z.C. Deng, T.J. Lu, Structural modeling of sandwich structures with lightweight cellular cores, Acta Mech. Sin. 23 (2007) 545–559.
[39] H.G. Allen, Analysis and Design of Structural Sandwich Panels, Pergamon Press, Oxford, 1969.
[40] C.G. Boay, Y.C. Wee, Coupling effects in bending, buckling and free vibration of generally laminated composite beams, Compos. Sci. Technol. 68 (2008) 1664–1670.
[41] M. Eisenberger, H. Abramovich, O. Shulepov, Dynamic stiffness analysis of laminated beams using a first order shear deformation theory, Compos. Struct. 31 (1995) 265–271.
[42] M. Tahani, Analysis of laminated composite beams using layerwise displacement

theories, Compos. Struct. 79 (2007) 535–547.
[43] R.P. Shimpi, A.V. Ainapure, Free vibration analysis of two layered cross-ply laminated beams using layer-wise trigonometric shear deformation theory, J. Reinf. Plast. Compos. 21 (2002) 1477–1492.
[44] P.B. Xavier, C.H. Chew, K.H. Lee, An improved zig-zag model for the vibration of soft-cored unsymmetric sandwich beams, Compos. Eng. 4 (1994) 549–564.
[45] H. Youzera, S.A. Meftah, N. Challamel, A. Tounsi, Nonlinear damping and forced vibration analysis of laminated composite beams, Compos. Part B - Eng. 43 (2012) 1147–1154.
[46] S.P. Timoshenko, On the correction for shear of the differential equation for transverse vibrations of prismatic bars, Philos. Mag. Ser. 6 (1921) 744–746.
[47] S.P. Timoshenko, On the transverse vibrations of bars of uniform cross-section, Philos. Mag. Ser. 43 (1922) 125–131.
[48] V.S. Deshpande, N.A. Fleck, Collapse of truss core sandwich beams in 3-point bending, Int. J. Solids Struct. 38 (2001) 6275–6305.
[49] V.S. Deshpande, N.A. Fleck, M.F. Ashby, Effective properties of the octet-truss lattice material, J. Mech. Phys. Solids 49 (2001) 1747–1769.
[50] T. Liu, Z.C. Deng, T.J. Lu, Analytical modeling and finite element simulation of the plastic collapse of sandwich beams with pin-reinforced foam cores, Int. J. Solids Struct. 45 (2008) 5127–5151.
[51] R. Hill, Elastic properties of reinforced solids: some theoretical principles, J. Mech. Phys. Solids 11 (1963) 357–372.